Ultra high resolution science data extraction for the Gravity Probe-B gyro and telescope

Richard A. Van Patten, Ray DiEsposti, John V. Breakwell

Department of Aeronautics and Astronautics, Stanford University
Stanford, California 94305

Abstract

In 1960, Leonard Schiff predicted, using Einstein's General Theory of Relativity, that a gyroscope in orbit about the Earth would experience a precession of its spin axis relative to the "fixed stars". Two relativistic precessions are predicted: a "geodetic" precession associated with the orbital motion of the gyro about the Earth, and a "motional" precession due to the Earth's rotation. For a gyro in a 650 km altitude polar orbit with its spin axis initially pointed towards an inertial reference, in this case the star Rigel, and lying in the orbital plane, the geodetic precession is 6.6 arcsec/yr north, and the motional precession is 0.042 arcsec/yr east. This scenario is illustrated in Figure 1.

To detect these relativistic drifts, a gyro is currently being developed whose absolute Newtonian drift rates are less than 10^{-3} arcsec/yr. Even with such a "perfect" gyro, however, the question arises: Can the relativistic drifts be detected in the presence of random measurement noise, and other error sources such as satellite attitude control system errors, Rigel proper motion uncertainty, drifts due to gyro suspension forces, drift of electronic parameters such as instrument scale factors due to thermal effects, etc.? This paper describes an all-digital data flow simulation that demonstrates the Kalman Filter data reduction process for detection of the relativistic drifts. The simulation demonstrates successful optimal estimation of the relativity effects in the presence of the expected measurement noise and consistent with the experiment lifetime, and the other above-mentioned effects.

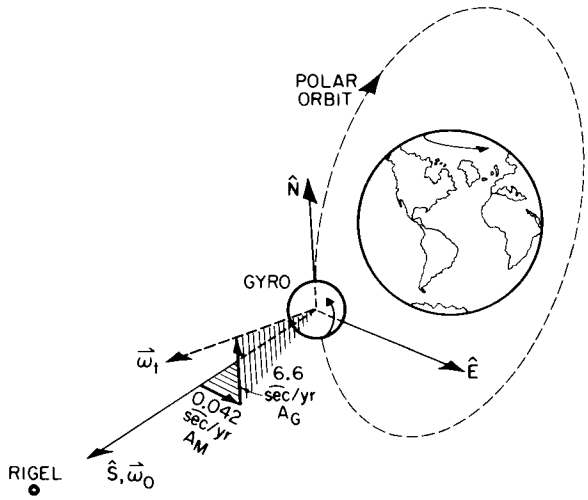

- o 650 km polar orbit
- o line-of-sight to Rigel ~ in orbital plane
- o telescope/spacecraft pointed nominally at Rigel and rolling about line-of-sight to Rigel
- o rotor spin axis towards Rigel
- o 1 SQUID loop per gyro

Figure 1: Scenario for the Gravity Probe-B Science Mission

List of symbols

$\hat{S}$, $\hat{E}$, $\hat{N}$	- Orthogonal basis for inertial axis system with $\hat{S}$ along the direction of Rigel, $\hat{E}$ in the eastward direction and parallel to the equatorial plane
$\vec{\omega}_o$	- Initial angular velocity vector of gyro rotor
$\vec{\omega}_t$	- Angular velocity vector of rotor at time t
ϕ	- Roll angle of satellite, where roll is about the line-of-sight to Rigel
$x(n)$	- State vector at time $t_n = nT$, where T is the sample period
$\Phi(n)$	- State transition matrix at time t_n
$G(n)$	- Input matrix at time t_n
$v(n)$	- State process noise and input vector at time t_n
$z(n)$	- Measurement vector at time t_n
$A(n)$	- Measurement matrix at time t_n
$n(n)$	- Measurement noise at time t_n

$\hat{x}(n)$ - State estimate at time t_n
$P(n)$ - State covariance matrix at time t_n
$R_n(i)$ - Measurement noise covariance at time t_i
$R_v^n(i)$ - State process noise covariance at time t_i
$\bar{v}(n)$ - Mean of process noise. Also can be a driving input process.
$J(n)$ - Performance function
$\bar{x}(o)$ - A priori initial state estimate
$M(o)$ - A priori initial state covariance
$y_G(t)$ - SQUID magnetometer gyro measurements
$y_T(t)$ - Telescope measurements
$\hat{b}_1$, $\hat{b}_2$, $\hat{b}_3$ - Orthogonal basis for axis system fixed in the satellite with $\hat{b}_3$ along the direction of Rigel
θ_1, θ_2 - Telescope pointing errors, ~30 milliarcsec
EW, NS - Inertial deviations of rotor spin axis from the $\hat{S}$ direction along the directions $\hat{E}$ and $\hat{N}$, respectively
C_G - SQUID (gyro) scale factor
C_T - Telescope scale factor
δ - Instantaneous dither angle
Δ - Amplitude of dithering motion
ω_δ - Frequency of dither
ω_r - Spacecraft roll frequency (10 minute roll period)
b - Measurement bias parameter
n_G, n_T - SQUID (gyro) and telescope noise, respective
$y(t)$ - Gyro measurement minus telescope measurement
n - Gyro noise plus telescope noise, predominantly SQUID (gyro) noise
K_T - Telescope scale adjusting factor
$\mathscr{y}_G(t)$, $\mathscr{y}_T(t)$ - Filtered SQUID (gyro) and telescope measurement signals
$H(x_n)$ - Measurement function of state

Parameters of EW rotor spin axis deviation:
- EW_o - Initial EW spin axis misalignment
- EW_G - Sensitivity of EW deviation with respect to geodetic relativity coefficient
- A_G - Geodetic relativity coefficient = 6.602 arcsec/yr
- EW_M - Sensitivity of EW deviation with respect to motional relativity coefficient
- A_M - Motional relativity coefficient = 0.04182 arcsec/yr
- PM_{EW} - Apparent EW deviation due to Rigel proper motion
- EW_{ann} - Apparent EW deviation due to aberration of starlight due to Earth's motion about Sun
- EW_{orb} - Apparent EW deviation due to aberration of starlight due to satellite's motion about Earth

Parameters of NS rotor spin deviation are similar to those of EW

States of the state vector x(n):
- ξ - Low-pass pre-filter state
- η - Measurement noise shaping filter state
- C_G - SQUID (gyro) scale factor
- ϕ - Satellite roll angle
- A_D - Amplitude of residual dither signal
- b - Measurement bias parameter
- A_G - Geodetic relativity coefficient
- A_M - Motional relativity coefficient
- PM_{EW} - Proper motion of Rigel along the $\hat{E}$ direction
- PM_{NS} - Proper motion of Rigel along the $\hat{N}$ direction
- EW_o - Initial EW spin axis misalignment
- NS_o - Initial NS spin axis misalignment
- ε - Apparent deviation due to parallax resulting from Earth's orbit about the Sun

$\mathscr{y}(t)$ - Filtered gyro measurement minus telescope measurement
a_0, a_1, b_1 - Low-pass pre-filter recursion coefficients
$w(n)$ - Uniformly distributed, uncorrelated random numbers (noise) at time t_n
c_0, c_1, d_1 - Measurement noise power spectrum shaping filter coefficients
$H_x(x(n))$ - Gradient vector of partial derivatives evaluated at state x(n), time t_n
$$= \left(\frac{\partial H}{\partial C_G}, \frac{\partial H}{\partial \phi}, \cdots, \frac{\partial H}{\partial \varepsilon}\right)\Bigg|_{x_n}$$
σ_{A_G} - Expected 1-sigma estimation error in A_G
= Square root of 7^{th} diagonal element of state covariance matrix
σ_{A_M} - Expected 1-sigma estimation error in A_M
= Square root of 8^{th} diagonal element of state covariance matrix
$H(s)$ - Low-pass pre-filter transfer function
$H_s(f)$ - SQUID measurement noise shaping filter

Introduction

The Stanford Relativity Gyroscope Experiment (Gravity Probe-B), will use four superconducting electrostatically suspended spherical gyros carried in a drag-free Earth satellite with spin axes nominally aligned with Rigel. Each spin orientation with respect to the line-of-sight to Rigel is measured using a SQUID magnetometer. This gives the direction of the London magnetic moment (which is along the gyro spin axis) compared to the readout of a telescope pointed nominally at Rigel. The satellite rolls about the line-of-sight to Rigel with a period of 10 minutes. By rolling about the line-of-sight, measurement signal contribution due to relativistic precessions become modulated at roll frequency, and can thus be separated from low frequency drift errors characteristic of 1/f SQUID noise.

To reduce error, the scale factors of the gyro and telescope readouts should be matched to about 2%. We plan to apply a low frequency, low amplitude, dithering command to the attitude control pointing system. This introduces a signal component at dither frequency which can be separated from the main signal and used in a feedback loop to adjust the telescope scale factor to match the gyro scale factor.

Recently a full Kalman Filter model was developed to handle the data reduction. Using "true" state values, the measurement model, and the state dynamic model, simulated measurement data, with added random noise was generated. This simulated data was fed into the Kalman Filter, whose output was the state estimate (which included the relativity effects) and state covariance.

The results agree well with the previous work of R. Vassar, J. V. Breakwell, C. W. F. Everitt and R. A. Van Patten.[1,2]

Included in the Kalman Filter model are the following:

1) A low-pass analog pre-sampling filter modeled as an equivalent discrete-time digital filter (one state).

2) Estimation and feedback of a sinusoidal dither signal to keep the net telescope scale factor matched to the gyro scale factor to within ~2% (one state).

3) A SQUID noise shaping filter (one state) designed to match projected power spectrum data at both roll frequency and dither frequency (the only frequencies of interest).

4) Ten additional states as follows:
   * Gyro scale factor
   * Spacecraft roll angle
   * Body fixed bias
   * Geodetic relativity coefficient
   * Motional relativity coefficient
   * East-west proper motion of Rigel
   * North-south proper motion of Rigel
   * Initial east-west gyro spin axis misalignment
   * Initial north-south gyro spin axis misalignment
   * Parallax of Rigel due to Earth's orbit about the Sun

5) The following are treated as "known" effects and permit self-calibration of the readout scale factor:
   * Orbital aberration of starlight
   * Annual aberration of starlight

6) Only time, orbital parameters and roll angle are updated during occultation of Rigel by Earth.

Note: An alternative and slightly simpler Kalman Filter would consider the differences [geodetic - northward proper motion] and [motional - eastward proper motion] rather than four separate states. The accuracy of determination of the relativity coefficients is of course limited by the knowledge of Rigel's proper motion.

Kalman Filter for data reduction

Given measurement data $z(n)$, $n=0,1,2,\ldots$, and a discrete-time mathematical model of a physical process which relates some quantities of interest $x(n)$, called states, to the measurements according to:

$$x(n+1) = \Phi(n)\, x(n) + G(n)\, v(n) \qquad (1)$$

$$z(n) = A(n)\, x(n) + n(n) \quad , \qquad (2)$$

the function of Kalman Filter data processing is to provide state estimates, $\hat{x}(n)$, from measurements $z(n)$. See block diagram Figure 2.

Figure 2: Data reduction by Kalman filtering

The state transition, input, and measurement matrices $\Phi(n)$, $G(n)$, and $A(n)$ respectively, $n=0,1,2,\ldots$ are assumed known. The quantity $n(n)$ is measurement sensor noise and $v(n)$ corresponds to state process noise which is included to account for inaccuracies in state dynamics modeling.

The statistics of the noise processes (assumed uncorrelated) are assumed known and given by:

$$E\{n(i)\, n^T(j)\} = \begin{cases} R_n(i), & i = j \\ 0, & i \neq j \end{cases} \tag{3}$$

$$E\left\{(v(i)-\bar{v}(i))(v(j)-\bar{v}(j))^T\right\} = \begin{cases} R_v(i), & i=j \\ 0, & i\neq j \end{cases} \tag{4}$$

$$E\{n(n)\} = 0, \quad E\{v(n)\} = \bar{v}(n), \quad E\{n(n)\left(v(n) - \bar{v}(n)\right)^T\} = 0 \tag{5}$$

Kalman Filter data processing algorithms are derived by minimizing the weighted sum-of-squares error performance function:

$$J(n) = \left(x(0) - \bar{x}(0)\right)^T M(0)^{-1} \left(x(0) - \bar{x}(0)\right) + \sum_{i=0}^{n} \{\left(A(i)\, x(i) - z(i)\right)^T R_n(i)^{-1}\left(A(i)\, x(i) - z(i)\right) + \left(v(i) - \bar{v}(i)\right)^T R_v(i)^{-1}\left(v(i) - \bar{v}(i)\right)\}$$

It can be shown[3] that minimization of J with respect to the unknown states $x(i)$ yields the following recursive algorithms for the state estimate $\hat{x}(n)$[4]:

$$\hat{x}(n) = \bar{x}(n) + MA^T \left(AMA^T + R_n\right)^{-1} \left(z(n) - A\bar{x}(n)\right) \tag{6}$$

$$P(n) = M(n) - M(n)\, A^T (AMA^T + R_n)^{-1}\, A\, M(n) \tag{7}$$

$$\bar{x}(n+1) = \Phi\, \hat{x}(n) + G\bar{v}(n) \tag{8}$$

$$M(n+1) = \Phi\, P(n)\, \Phi^T + G\, R_v\, G^T \tag{9}$$

It can be shown that the matrix $P(n)$ is the state covariance matrix defined by $P(n) = E\{\left(x(n) - \hat{x}(n)\right)\left(x(n) - \hat{x}(n)\right)^T\}$.

The diagonal elements of $P(n)$ correspond to a 1-sigma variance of the estimate error and thus provide a theoretical indication of estimate accuracy.

The algorithms (equations (6) to (9)) are started by assuming an a priori initial state estimate $\bar{x}(o)$ and an initial state covariance $M(o)$ which corresponds to the uncertainty in the initial state estimate. The algorithms are propagated forward in time with each new measurement $z(n)$. For the Gravity Probe-B (GP-B) data flow simulation, the processing algorithms (equations (6) - (9)) are implemented in the numerically accurate square root form[3].

Development of a mathematical model for the GP-B measurements

The two primary measurements for data reduction of the GP-B experiment are the SQUID magnetometer and telescope measurements. Shown in Figure 3(a) is the spacecraft pointed nominally towards the star Rigel (inertial reference) and rolling about the line-of-sight to Rigel. The spacecraft is commanded to point to Rigel but due to limitations of the attitude control system, non-negligible pointing errors are measured by the telescope as shown in Figure 3(b). The SQUID magnetometer measurement is proportional to the angle between the gyro spin vector $\vec{\omega}_t$ and the SQUID loop plane, which is fixed in the spacecraft; see Figure 3(c). General relativity predicts[5] that the gyro spin axis will precess 6.6 arcsec/yr in the Northward direction due to the Geodetic Effect and 0.042 arcsec/yr in the Eastward direction due to the Motional Effect. The purpose of the experiment is to detect these relativistic effects. The spacecraft is also made to undergo a small amplitude sinusoidal dithering motion about satellite body axis $\hat{b}2$. As will be shown, this dithering motion serves to provide a signal for matching the gyro and telescope scale factors to about 2%. The gyro (SQUID) and telescope measurements can be shown to be given by[2]:

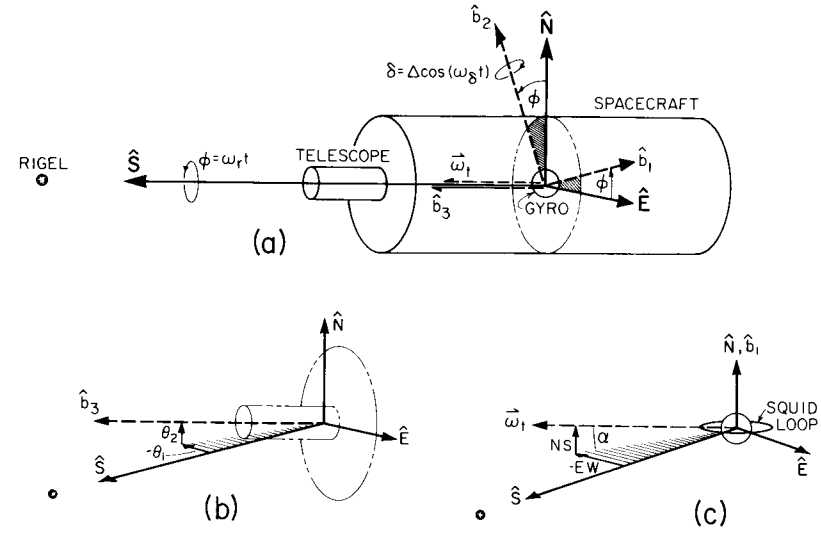

Figure 3: Spacecraft orientation and telescope and gyro measurements

Gyro: $$y_G(t) = C_G(EW \cos\phi + NS \sin\phi) + C_G\,\delta + b + C_G(\theta_1 \cos\phi + \theta_2 \sin\phi) + n_G \quad (10)$$

Telescope: $$y_T(t) = C_T(\theta_1 \cos\phi + \theta_2 \sin\phi) + C_T\,\delta + n_T \quad (11)$$

$$y(t) = C_G(EW \cos\phi + NS \sin\phi) + (C_G - C_T)\,\delta + (C_G - C_T)(\theta_1 \cos\phi + \theta_2 \sin\phi) + b + n \quad (12)$$

Note the dependence on the spacecraft roll angle ϕ and the appearance of the dithering motion δ in both the gyro and the telescope signals. The gyro spin axis deviations EW and NS are modeled by initial misalignments EW_O and NS_O, relativity drift effects, and inertial corrections due to the known effects of aberration of starlight, parallax, and Rigel proper motion. In addition, though not considered in this simulation, it may be necessary to model other effects such as polhoding of the gyro rotor, torque induced drift, bending of starlight, and Earth oblateness effects. These effects were considered in previous error analyses.[2,6] Note that the spacecraft pointing error appears in the gyro measurements, equation (10). To recover the inertial reference, the telescope signal is subtracted from the gyro signal.(12) Notice that the pointing errors θ_1, and θ_2 and the dithering motion δ corrupt the measurement (do not drop out) unless the scale factors are matched; $C_G = C_T$. As will be shown later, the residual dither signal $(C_G - C_T)\delta$ can be used in a feedback scheme to adjust the telescope scale factor.

Data flow instrumentation and data reduction simulation

The data reduction simulation considered the configuration depicted in Figure 4, which is

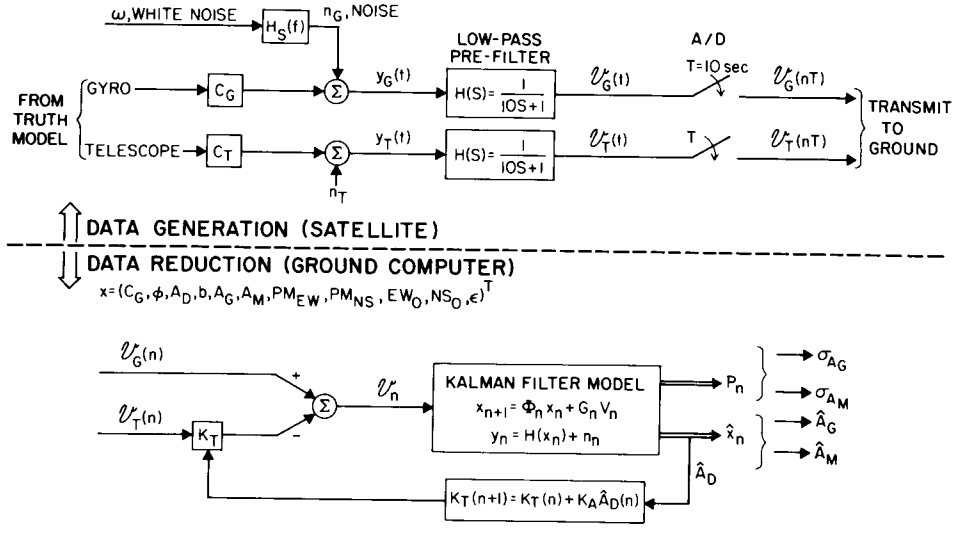

Figure 4: Data flow simulation and data reduction

representative of the most basic set-up. Both gyro and telescope signals are passed through low-pass filters before sampling to decrease the effect of aliasing of high frequency noise. After sampling, the gyro and telescope data are transmitted to ground where the data processing occurs. A scale adjusting factor K_T is introduced to the telescope data on ground. The Kalman Filter thus sees a residual dither signal contribution of $(C_G - K_T C_T) \Delta \cos(\omega_\delta t) \triangleq A_D \cos(\omega_\delta t)$. Separating the dither signal from the other frequencies, a feedback law is implemented, based on the estimate $\hat{A}_D$, to match the scale factors, i.e., $K_T \to C_G/C_T$. The actual study consisted of an all-digital simulation. Truth model measurement data was generated digitally using an assumed "true" state value x and measurement equations (10) and (11). The low-pass analog filtering process H(s): $y \to v$ was simulated by an equivalent discrete-time digital filter. A noise shaping filter[7] was added to approximate SQUID noise power spectrum data projected from previous experimental work.[8] The generated data, $v_G(n)$ and $v_T(n)$, was thus submitted to the Kalman Filter algorithms. The objective of the data processing is to extract, as accurately as possible, the assumed true state x. The state estimate $\hat{x}$ and covariance P serve as actual and theoretical, respectively, indicators of data reduction performance.

Manipulation of the mathematical model into a form compatible for Kalman filtering

Before data processing can be applied, the measurement equations (10) and (11) must be manipulated into the general form of equations (1)-(5). The mathematical model consists of the following:

$$y(n) \triangleq y_G(n) - y_T(n) = H(x(n)) + n(n) \tag{13}$$

where $H(x_n) = C_G(EW \cos\phi + NS \sin\phi) + A_D \cos(\omega_\delta t) + b$

and $EW = EW_o + EW_G A_G + EW_M A_M + PM_{EW} t + EW_{ann} + EW_{orb}$

$NS = NS_o + NS_G A_G + NS_M A_M + PM_{NS} t + NS_{ann} + NS_{orb}$

$$x(n+1) = \Phi'(n)\, x(n) + G' v'(n) \tag{14}$$

where $\Phi' = I_{11x11}$ for state x defined as

$x \triangleq (C_G, \phi, A_D, b, A_G, A_M, PM_{EW}, PM_{NS}, EW_o\ NS_o, \varepsilon)^T$

$$\mathscr{v}(n) \triangleq \mathscr{v}_G(n) - \mathscr{v}_T(n) \tag{15}$$

$$= -b_1\, \mathscr{v}(n-1) + a_0 y(n) + a_1 y(n-1)$$

Low-pass pre-filter with cut-off at $\omega_c = 0.10$ rad/sec
With $b_1 = -1/3$, $a_0 = a_1 = 1/3$

$$n(n) = -d_1\, n(n-1) + c_0 \omega(n) + c_1 \omega(n-1) \tag{16}$$

Noise power spectrum shaping filter
With $d_1 = -0.71915$, $c_0 = c_1 = 0.14042$

First, linearize equation (13) by Taylor's series expansion:

$$y(n) \approx H(\bar{x}(n)) + H_x(\bar{x}(n))\ (x(n) - \bar{x}(n)) + \ldots + n(n) \tag{13}'$$

Equations (15) and (16) can be realized in state space form as:

$$\xi(n+1) = -a_1/a_0\ \xi(n) + 1/a_0\ \mathscr{v}(n) \tag{15}'$$
$$\mathscr{v}(n) = (a_1 - a_0 b_1)\ \xi(n) + a_0 y(n)$$

$$\eta(n+1) = -d_1\ \eta(n) + \omega(n) \tag{16}'$$
$$n(n) = (c_1 - c_0 d_1)\ \eta(n) + c_0\ \omega(n)$$

Substituting (16)' into (13)' and then (13)' into (15)':

$$\Rightarrow \mathscr{v}(n) = (a_1 - a_0 b_1)\ \xi(n) + a_0 \{H(\bar{x}(n)) + H_x(\bar{x}(n))\ (x(n) - \bar{x}(n)) + (c_1 - c_0 d_1)\ \eta(n) + c_0\ \omega(n)\}$$

$$\Rightarrow \mathscr{v}(n) - a_0[H(\bar{x}(n)) - H_x(\bar{x}(n)) \cdot \bar{x}(n)] = [a_0(c_1 - c_0 d_1) \vdots (a_1 - a_0 b_1) \vdots a_0 H_x(\bar{x}(n))] \begin{bmatrix} \eta(n) \\ \xi(n) \\ \bar{x}(n) \end{bmatrix} + a_0 c_0 \omega(n) \tag{17}$$

Equation (17), which will become the new measurement equation, contains the noise term $a_0 c_0\ \omega(n)$ which is correlated with the process noise term in equation (16)'. This violates the uncorrelated assumption of equation (5). To remove the correlation, subtact $\frac{1}{a_0 c_0} \times$ (17) from (16)' :

$$\eta(n+1) = -\frac{1}{a_0 c_0}(a_1 - a_0 b_1)\,\xi(n) - \frac{c_1}{c_0}\,\eta(n) - \frac{1}{c_0} H_x(\bar{x}(n)) \cdot x(n) + \frac{1}{a_0 c_0}\left[\mathscr{v}(n) - a_0\left(H(\bar{x}(n)) - H_x(\bar{x}(n)) \cdot \bar{x}(n)\right)\right] \tag{16}"$$

Equations (15)' and (16)" can be augmented to (14):

$$\begin{bmatrix} \eta(n+1) \\ \xi(n+1) \\ \hline x(n+1) \end{bmatrix} = \left[\begin{array}{cc|c} -\frac{c_1}{c_0} & -\frac{1}{a_0 c_0}(a_1 - a_0 b_1) & -\frac{1}{c_0} H_x(\bar{x}(n)) \\ 0 & -\frac{a_1}{a_0} & 0 \\ \hline 0 & 0 & I_{11x11} \end{array}\right] \begin{bmatrix} \eta(n) \\ \xi(n) \\ \hline x(n) \end{bmatrix} + \begin{bmatrix} \frac{1}{a_0 c_0}\left[\mathscr{v}(n) - a_0\left(H(\bar{x}(n)) - H_x(\bar{x}(n)) \cdot \bar{x}(n)\right)\right] \\ \frac{1}{a_0}\,\mathscr{v}(n) \\ G'\,v'(n) \end{bmatrix} \tag{18}$$

Equations (17) and (18) are now in the general form of equations (1)-(5), with:

$$\Phi(n) = \begin{bmatrix} -\frac{c_1}{c_0} & -\frac{1}{a_0 c_0}(a_1 - a_0 b_1) & -\frac{1}{c_0} H_x(\bar{x}(n)) \\ 0 & -\frac{a_1}{a_0} & 0 \\ 0 & 0 & I_{11x11} \end{bmatrix}, \text{ and} \tag{19}$$

$$Gv(n) = \begin{bmatrix} \frac{1}{a_0 c_0}\left[\mathscr{v}(n) - a_0\left(H(\bar{x}(n)) - H_x(\bar{x}(n)) \cdot \bar{x}(n)\right)\right] \\ \frac{1}{a_0}\,\mathscr{v}(n) \\ G'v'(n) \end{bmatrix} \tag{20}$$

$$A(n) = \left[a_0(c_1 - c_0 d_1) \vdots (a_1 - a_0 b_1) \vdots a_0\, H_x(\bar{x}(n))\right] \tag{21}$$

$$z(n) = \mathscr{v}(n) - a_0\left[H(\bar{x}(n)) - H_x(\bar{x}(n)) \cdot \bar{x}(n)\right] \tag{22}$$

$$n(n) = a_0 c_0\,\omega(n) \tag{23}$$

The Kalman Filter data processing algorithms, equations (6)-(9) are applied using the above defined elements. The a priori state estimate at time t_n, $\bar{x}(n)$, as given by equation (8), is used in equations (19) to (22) to evaluate the measurement function, $H(\bar{x}(n))$, and the measurement gradient vector, $H_x(\bar{x}(n))$.

Results

Simulated measurement data was generated using equations (10) and (11) and an assumed "true" state, x. Figure 5 shows the simulated gyro-telescope signal. The sinusoidal nature of the signal due to spacecraft roll and the modulation due to orbital aberration of starlight are readily apparent. As illustrated in Figure 4, random measurement noise was added to the signal prior to data processing. Shown in Figure 6 is a time recording of the measurement noise. The noise was generated by passing uniformly distributed, uncorrelated random numbers through a third-order digital recursion. The recursion was designed to approximate experimental power spectrum and noise amplitude data of an advanced D C SQUID magnetometer of the N.B.S. type. The measurement data was passed through a low-pass filter, as shown in Figure 4, before being submitted to the Kalman Filter. The outputs of the Kalman Filter are the state estimates. In particular, we are interested in how well the relativity effects can be extracted from the measurement data. Shown in Figure 7 is a time history of the geodetic coefficient estimate. The truth model value was taken at 6.602 arc sec/yr., and the estimate error is seen to fall to 5.7 marcsec/yr (0.086%) after 6 months of data processing. The motional coefficient estimate appears in Figure 8. The true value is 0.04182 arcsec/yr. For this run,zero proper motion for Rigel was assumed. The estimate error after 6 months is seen to be 2.59 marcsec/yr. These results compare well with previous error analyses. Figure 9 and Figure 10 show the estimated covariance time histories, for June and September launches, respectively, for the relativity effects as determined by

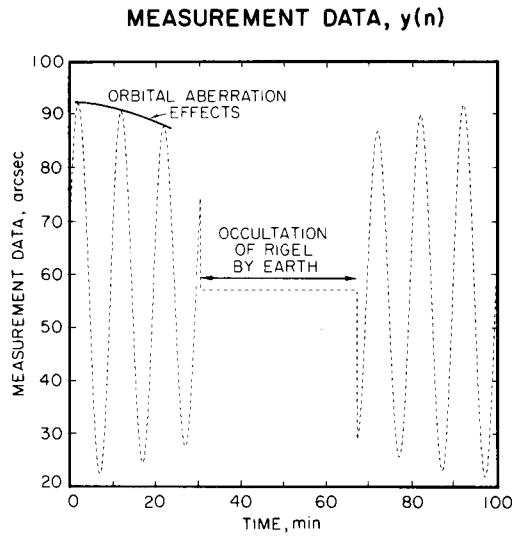

Figure 5: Gyro minus telescope simulated measurement data

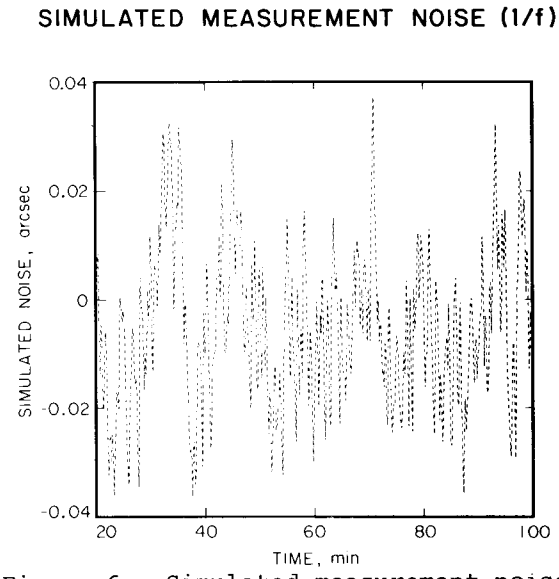

Figure 6: Simulated measurement noise

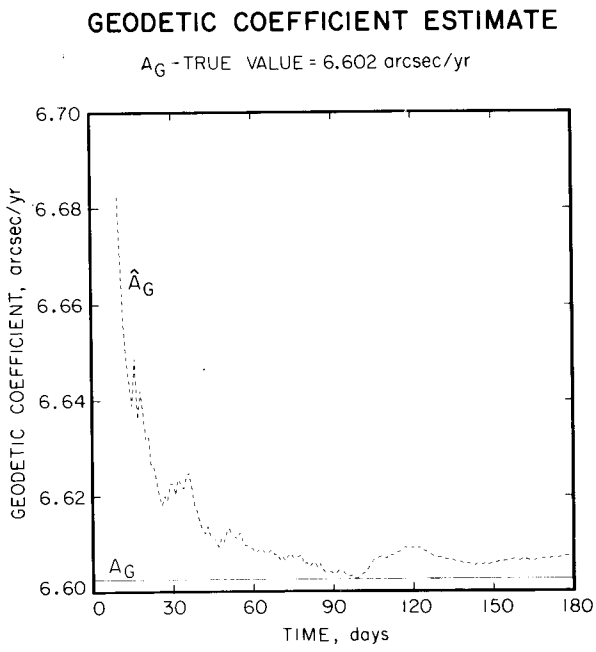

Figure 7: Time history of geodetic coefficient estimate

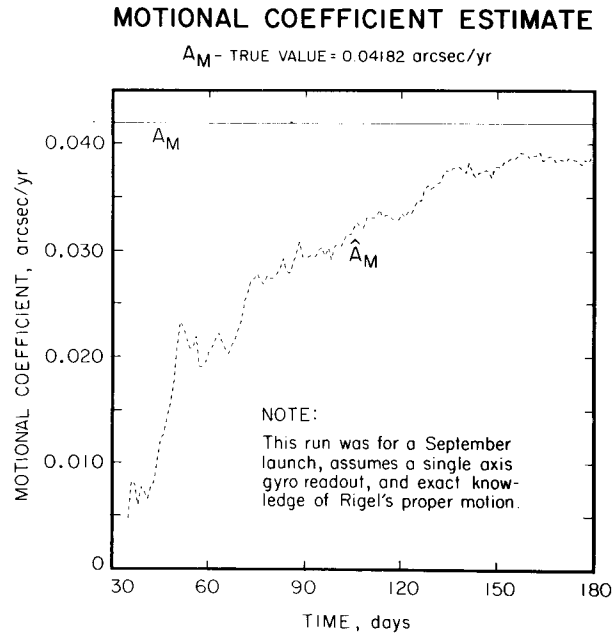

Figure 8: Time history of motional coefficient estimate

R. Vassar[2] in 1982. Based on Vassar's results,we decided to run a September launch case because the motional coefficient error after one year is seen to be less for a September versus a June launch. In an earlier one year run which assumed a June launch and a somewhat higher noise level (3.7 to 1 noise equivalent angle), the geodetic estimate error was approximately 1 marcsec (0.015%) after a 12 month simulation. The motional estimate error was 2.2 marcsec/yr after 12 months. The results of the earlier run also compare well with Vassar's covariance analyses.

Conclusion

Successful extraction of the geodetic effect and the motional effect was demonstrated after separate six and twelve month simulation runs. Extension of the current run from 6 to 12 months (48 hours of CPU time on a VAX 11-780) should yield further improvement in the estimate accuracy. The extended run was in progress at the time of this publication deadline.

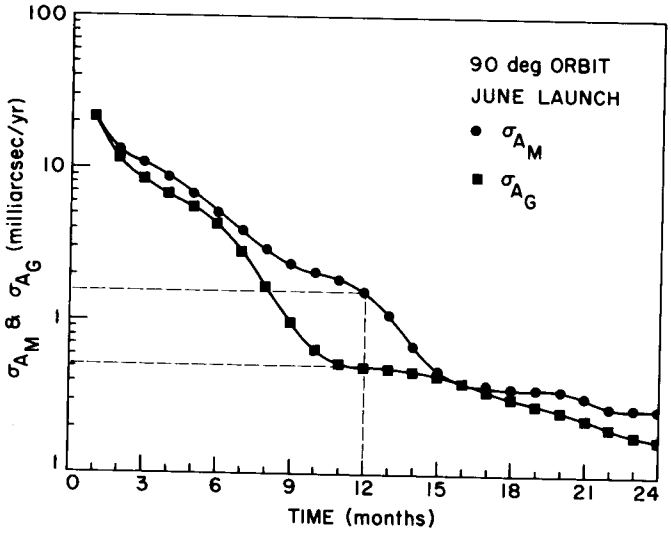

Figure 9: Time history of σ_{A_M} and σ_{A_G} for a 90 deg. orbit, June launch

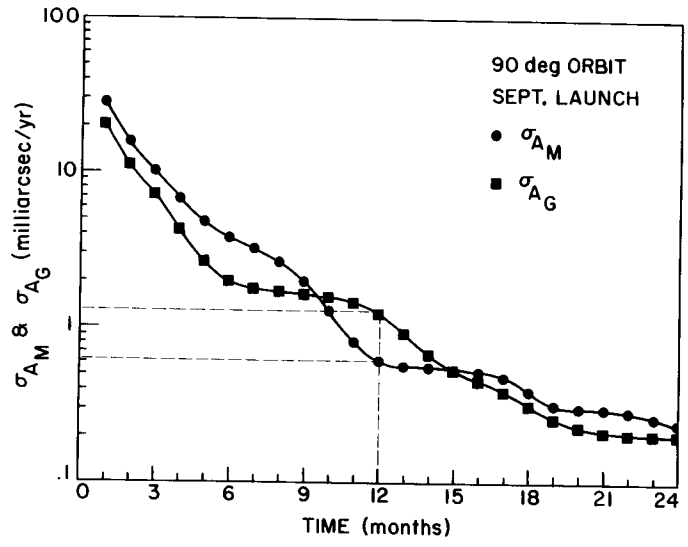

Figure 10: Time history of σ_{A_M} and σ_{A_G} for a 90 deg. orbit, Sept.launch

Future studies will include fine tuning the Kalman Filter, and Monte Carlo type simulations that evaluate the effects of parameter variation. We also plan to selectively insert critical hardware elements into the simulation.

We have recently obtained access to the Cray XMP 48 Super Computer at NASA Ames Research Center for a trial run. With the speed advantage of the Cray one year simulations are obtainable over night rather than the two to four weeks required on the VAX.

Acknowledgements

We acknowledge the following persons at NASA Ames for their assistance and encouragement in obtaining access to the Cray XMP 48 Super Computer for a trial run: Ramsey Malugin, Lou Peach, Catherine Schulbach.

We also acknowledge the helpful support of the following employees of Zeroone Systems Inc. (Cray Operations): John Avila, Sue Cox.

References

1) Vassar, R., Breakwell, J. V., Everitt, C. W. F., Van Patten, R. A., "Orbit Selection for the Stanford Relativity Gyroscope Experiment, "J. Spacecraft & Rockets, Vol. 19, no. 1, pp. 66-71, Jan.-Feb. 1982

2) Vassar, R., "Error Analysis for the Stanford Relativity Gyroscope Experiment", Stanford University, Ph.D. thesis, 1982

3) Bierman, G. J., "Factorization Methods for Discrete Sequential Estimation", Academic Press, New York, NY 1977

4) Franklin, G. F., and Powell, J. D., "Digital Control of Dynamic Systems", Addison-Wesley, Reading, Mass., 1981

5) Schiff, L. I., "Possible New Experimental Test of General Relativity Theory", Physical Review Letters, Vol.4, No. 5, March 1, 1960, 215-217

6) Duhamel, T. G., "Contributions to the Error Analysis in the Relativity Gyroscope Experiment", Stanford University, Ph.D. thesis, 1984

7) Maybeck, P. S., "Stochastic Models, Estimation and Control, Volume 1", Academic Press, New York, NY 1979

8) Anderson, J. T. and Cabrera, B., "Integration of SQUID 1/f Noise and its Application to a Superconducting Gyroscope", J. Physique 39, C6-1210-C6-1212